Aziz *et al. EURASIP Journal on Wireless Communications and Networking* (2016) 2016:189
DOI 10.1186/s13638-016-0683-4

EURASIP Journal on Wireless Communications and Networking

RESEARCH Open Access

A new DOA-based factor graph geolocation technique for detection of unknown radio wave emitter position using the first-order Taylor series approximation

Muhammad Reza Kahar Aziz[1,2*], Khoirul Anwar[1] and Tad Matsumoto[1,3]

Abstract

This paper proposes a new geolocation technique to improve the accuracy of the position estimate of a single unknown (anonymous) radio wave emitter. We consider a factor graph (FG)-based geolocation technique, where the input are the samples of direction-of-arrival (DOA) measurement results sent from the sensors. It is shown that the accuracy of the DOA-based FG geolocation algorithm can be improved by introducing approximated expressions for the mean and variance of the tangent and cotangent functions based on the first-order Taylor series (TS) at the tangent factor nodes of the FG. This paper also derives a closed-form expression of the Cramer-Rao lower bound (CRLB) for DOA-based geolocation, where the number of samples is taken into account. The proposed technique does not require high computational complexity because only mean and variance are to be exchanged between the nodes in the FG. It is shown that the position estimation accuracy with the proposed technique outperforms the conventional DOA-based least square (LS) technique and that the achieved root mean square error (RMSE) is very close to the theoretical CRLB.

Keywords: CRLB, DOA, Factor graphs, Geolocation, Taylor series

1 Introduction

Accurate wireless geolocation has received considerable attention in the past two decades [1] and is expected to play important roles in current and future wireless communications systems. This technology is the key to supporting location-based service applications, e.g., Emergency-911 (E-911), location-sensitive billing, smart transportation systems, vehicle navigation, fraud detection, people tracking, and public safety systems [1–3]. This paper proposes a new direction-of-arrival (DOA)-based factor graph (FG) geolocation technique to detect the position of a single unknown anonymous radio wave emitter (the terminology "anonymous" is omitted in the rest of the paper for simplicity), where to convert the measured DOA samples to the mean and variance of the tangent and cotangent functions, we utilize the first-order Taylor series (TS) approximation. The proposed technique is not only applicable for an unknown radio wave emitter, e.g., illegal radio wave emitter, but it is also applicable for common radio wave emitter position detection. The basic setup is shown in Fig. 1, where the FG is performed at the fusion center.

The FG is first applied on a geolocation technique in [4]. In the FG, the complexity is reduced because the global function factors into the products of several simple local functions, and the messages passed through the nodes are in the form of mean and variance, because of the Gaussianity assumption of the measured sample distribution [5–8]. The FG technique has been extended to incorporate not only DOA [6, 7] but also other information sources such as time of arrival (TOA) [8, 9], time difference of arrival (TDOA) [10], and received signal strength (RSS) [11], since the location of the unknown

*Correspondence: reza.kahar@jaist.ac.jp
[1] School of Information Science, Japan Advanced Institute of Science and Technology (JAIST), 1-1 Asahidai, Nomi-shi 923-1292, Japan
[2] Electrical Enginering Department, Institut Teknologi Sumatera (ITERA), Lampung Selatan 35365, Indonesia
Full list of author information is available at the end of the article

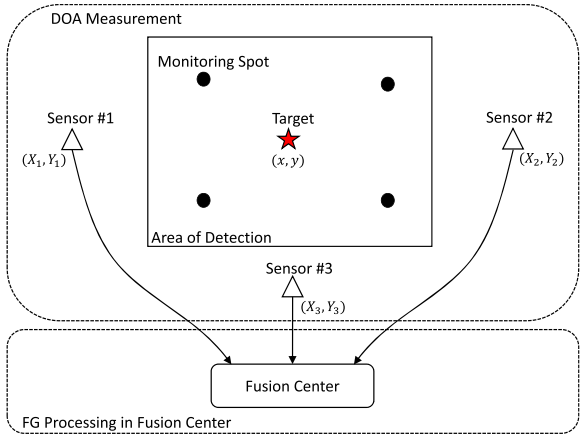

Fig. 1 Basic structure of FG-based unknown radio wave emitter detection describing a single target, four monitoring spots (in the case of RSS-based FG technique), three sensors, and fusion center

radio wave emitter can be estimated from them. In this paper, we use the terminology DOA instead of angle of arrival (AOA) for better expression.

DOA is used in this paper because it is measured by using either antenna arrays or a directional antenna without requiring perfect synchronization, time stamp, or transmit power information of a single unknown radio wave emitter [12, 13]. The other FG-based techniques, in contrast to the DOA-based techniques, e.g., TOA-based techniques, should perform perfect time synchronization among the sensors as well as between the sensors and the unknown emitter. The TDOA-based techniques can eliminate the necessity of the synchronization between the sensors and the emitter, but still, the sensors have to be accurately synchronized. Perfect synchronization is needed both in TOA and TDOA because the high velocity of the light, e.g., error of 1 μs, leads to error around 300 m [8]. Another difficulty arises in TOA-based geolocation techniques, where the TOA parameters cannot be measured from an unknown radio wave emitter because the time stamp information (time of departure (TOD) of the signal) of the transmitted signal from an unknown radio emitter is not available.

On the other hand, the major difficulty with the RSS-based technique is that it requires equal transmit power between the target and the test signal transmitted from the monitoring spots to gather the preliminary RSS map [11]. However, the transmit power of an unknown radio wave emitter is not available. The facts described above motivate us to use the DOA-based FG techniques to detect the position of the unknown radio emitter. The DOA-based FG techniques are also suitable in line-of-sight (LOS) and imperfect synchronization conditions.

1.1 Related work

A lot of work in DOA-based geolocation techniques have been proposed even since 30 years ago [14, 15]. However, it is quite recently that the FG-based techniques using DOA, TOA, TDOA, and RSS information were proposed, where the measurement data related to those parameters are used as the input to the algorithms. A joint TOA-DOA-based FG geolocation algorithm was proposed in [6], where the measured samples are efficiently used in FG to estimate the position accurately. Nevertheless, the joint TOA-DOA-based FG geolocation algorithm shown in [6] is still not fully correct because the message to be exchanged, the information of measurement error derived from the measurement results, enters the FG at an improper node as identified by [8].

The FG geolocation technique derived in [6] is improved in [7] as suggested in [8]. It also removes the necessity of measuring the TOA data from the joint TOA-DOA-based FG geolocation algorithm shown in [6] to obtain a simple DOA-based FG technique. After the DOA-based FG technique reaches a convergence point, the position estimate results are used as the initial position for the Gauss-Newton (GN) algorithm as the second step of the algorithm, the so-called factor graph-Gauss-Newton (FG-GN) geolocation technique in [7], to attain even higher accuracy.

We found that (1) The distance (r) is used in [7] as an argument of the tangent and cotangent functions, i.e., $\tan(r)$ and $\cot(r)$, which is obviously incorrect. Instead, the angle should be the argument of the tangent and cotangent functions, i.e., $\tan(\theta)$ and $\cot(\theta)$. (2) The factor node for collecting the samples is not available in the DOA-based FG geolocation techniques in [6, 7]. Moreover, the input parameter in [7] is r instead of θ. (3) The mean formula of tangent and cotangent function nodes [7] is not clearly described.

The Cramer-Rao lower bound (CRLB) is derived in [7], and the results of a series of simulations conducted to evaluate the accuracy of the DOA-based FG geolocation technique are shown also in [7] for the comparison purpose between CRLB and the root mean square error (RMSE) of DOA-based geolocation techniques, i.e., FG-GN, GN, and FG. However, the CRLB of the DOA-based technique shown in [7] does not take into account the influence of the sample number, and hence, the accuracy of the detection, when the number of the samples is large, is better than the CRLB, leading to the unusefulness of the comparison.

1.2 Contributions

In the FG-based geolocation techniques described above, each sensor performs DOA measurement and transmits samples to the fusion center. Only the mean and variance

of the DOA samples are used in the FG because of the Gaussianity assumption. The FG converts the angle information to the coordinate distance, referred to as relative distance, between the target and the sensor. The message passing takes place between the factor nodes and the variable nodes in the FG to obtain the target position estimate.

This paper provides clear understanding of the DOA-based geolocation techniques using FG, where the detail explanation of how the messages are updated at each node, and how the updated messages are exchanged between the nodes. The primary objectives of this paper are as follows: (A) We introduce a new set of formulas to be calculated at the tangent and cotangent factor nodes, to better approximate the mean and variance of the function values by utilizing the first-order TS expansion of the functions, so that the Gaussianity assumption still holds. (B) We derive the CRLB of the DOA-based geolocation technique taking into account the number of samples; hence, the accuracy of the new CRLB obtained by this paper is higher than that shown in [7]. (C) The results of a series of simulations are presented to evaluate the convergence property of the proposed technique, where the trajectory of the iterative estimation process is presented. Comparison between the RMSE of the proposed technique and the new CRLB is also provided. It is shown that the proposed algorithm can achieve close-CRLB accuracy, where the number of the samples, the number of the sensors, and the standard deviation of measurement error are used as a parameter.

The GN technique requires good initial position before it starts the iteration, while the proposed technique can start at any initial point. Therefore, it is not required to make a comparison between our proposed technique and the GN technique because we start the iteration from any arbitrary points. Also, since the detailed description of the algorithm for the DOA-based FG geolocation techniques presented in [6, 7] have improper expression as mentioned above in Section 1.1, this paper does not compare the accuracy of the proposed technique with that of [6] and [7]. Instead, the accuracy comparison is between the proposed technique and the DOA-based least square (LS) geolocation [16]. The FG we propose in this paper includes the DOA *measurement factor node* D_θ and *angle variable node* N_θ, as shown in Fig. 2, as in [8]. The two new nodes are proposed to emphasize that we need to calculate the mean and variance of DOA samples. It should be noted here that it is impossible to calculate variance with only one sample. It is also shown in this paper that with the proposed technique, the accuracy of the target position estimation outperforms the conventional DOA-based LS geolocation technique and the results are also very close to theoretical CRLB for the DOA-based geolocation.

2 System model

In general, the FG consists of the factor and variable nodes. In Fig. 2, the factor node is shown by a square, while the variable node by a circle. The factor node updates the messages forwarded from the connected variable nodes by using the specific simple local function, and the result is passed to the destination variable node. During the iteration, the messages sent from the source factor nodes are further combined in the variable node

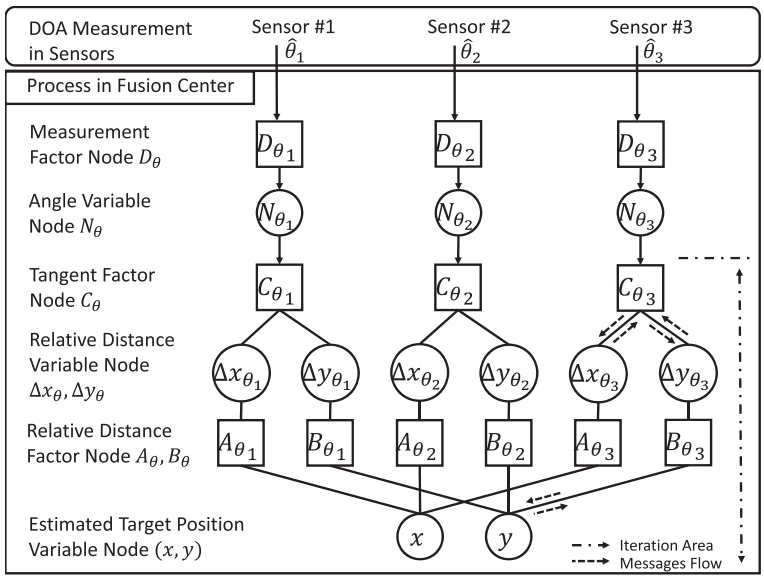

Fig. 2 The proposed DOA-based TS FG for geolocation technique

and passed back to the destination factor node for the next round of iteration. At the final iteration, the variable node combines the messages from all the connected factor nodes by using the sum-product algorithm.

Assume that the unknown radio wave emitter is located at coordinate position $\mathbf{x} = [x\ y]^T$, where T is the transpose function. Sensors are located at position $\mathbf{X}_i = [X_i\ Y_i]^T$, where i, $i = \{1, 2, \ldots, N\}$, is the sensor index. The orientation of the sensors is known to ensure that the sensors measure the angle with respect to the global coordinate system. The sensor to fusion center transmission is perfect via wired or wireless connections. $\Delta\mathbf{x}_{\theta_i} = [\Delta y_{\theta_i}\ \Delta x_{\theta_i}]^T$ is the relative distance between the position (X_i, Y_i) and target position (x, y), given by

$$\begin{bmatrix} \Delta x_{\theta_i} \\ \Delta y_{\theta_i} \end{bmatrix} = \begin{bmatrix} X_i \\ Y_i \end{bmatrix} - \begin{bmatrix} x \\ y \end{bmatrix} \tag{1}$$

with the θ_i being the true DOA; however, the measured samples are corrupted by error due to the spatial spread of the multipath component and impairments in measurement. The DOA measurement equation is then given by

$$\hat{\theta}_k = \theta + n_k, \quad k = \{1, 2, \ldots, K\}, \tag{2}$$

where k is the sample index. For notation simplicity, the sensor index i is omitted from the equations common to all the sensors, while it is included when needed, in the rest of the paper. It is reasonable to assume that n_k is independent identically distributed (i.i.d.) zero-mean Gaussian random variable. The Gaussianity assumption is used in this paper because of the accumulative effects of many independent factors, as in [6–8, 10, 11]; hence, the assumption is reasonable for many of the wireless parameter measurement-based techniques such as DOA, TOA [8], TDOA [10], and RSS-based FG technique [11]. Furthermore, it can simplify the total computational complexity. This Gaussianity assumption is also used for the TOA/DOA-based FG technique in [6] and the DOA-based FG technique in [7]. This paper also uses the same assumption. Then, $\hat{\theta}$ follows a normal distribution $\mathcal{N}(\theta, \sigma^2)$ having a probability density function $p(\hat{\theta})$ as

$$p(\hat{\theta}) = \frac{1}{\sqrt{2\pi}\sigma_\theta} \exp\left(\frac{-(\hat{\theta} - \theta)^2}{2\sigma_\theta^2}\right),$$

where the sample index is also omitted from the expression. However, each sensor does not know the needed values of θ and σ_θ. Hence, each sensor in the proposed DOA-based TS FG geolocation technique first calculates the mean $m_{D_\theta \to N_\theta}$ and the variance $\sigma^2_{D_\theta \to N_\theta}$ from the K-measured samples. The mark "$\to$" in the suffix indicates the message flow directions in the FG.

The node D_θ forwards the messages $(m_{D_\theta \to N_\theta}, \sigma^2_{D_\theta \to N_\theta})$ to the N_θ, and then, the messages $(m_{N_\theta \to C_\theta}, \sigma^2_{N_\theta \to C_\theta})$ are directly forwarded to the *tangent factor node* C_θ, where $m_{N_\theta \to C_\theta} = m_{D_\theta \to N_\theta}$ and $\sigma^2_{N_\theta \to C_\theta} = \sigma^2_{D_\theta \to N_\theta}$. The angle messages $(m_{N_\theta \to C_\theta}, \sigma^2_{N_\theta \to C_\theta})$ are converted to the relative distance messages $(m_{C_\theta \to \Delta x_\theta}, \sigma^2_{C_\theta \to \Delta x_\theta})$ and $(m_{C_\theta \to \Delta y_\theta}, \sigma^2_{C_\theta \to \Delta y_\theta})$ in the node C_θ. The relative distance in (1) in the (X, Y) coordinate and the true DOA θ are connected by the tangent and cotangent functions, as [6, 7]

$$\Delta y_\theta = \Delta x_\theta \cdot \tan(\theta), \tag{3}$$

$$\Delta x_\theta = \Delta y_\theta \cdot \cot(\theta). \tag{4}$$

Even though (3) and (4) are self-referenced point equations, which can be solved by iterative techniques, the iteration needs proper initialization of the mean and variance of the argument variables $\Delta\hat{x}_\theta$ and $\Delta\hat{y}_\theta$ which are corresponding to $\hat{x}$ and $\hat{y}$ by (1) and (2), where the detail of initializations are described in Section 5. We do not know the true values of θ, Δx_θ, Δy_θ, x, and y; however, the message needed in the FG is the mean and variance of samples $\hat{\theta}$, $\Delta x_{\hat{\theta}}$, $\Delta y_{\hat{\theta}}$, $\hat{x}$, and $\hat{y}$, which can be produced from the angle messages in the form of the mean and variance of samples $\hat{\theta}$, $(m_{D_\theta \to N_\theta}, \sigma^2_{D_\theta \to N_\theta})$. The details of the entire process are described in next section.

3 The proposed technique

The messages corresponding to Δy_θ and Δx_θ of (3) and (4), respectively, are the mean and variance, i.e., $(m_{C_\theta \to \Delta x_\theta}, \sigma^2_{C_\theta \to \Delta x_\theta})$ and $(m_{C_\theta \to \Delta y_\theta}, \sigma^2_{C_\theta \to \Delta y_\theta})$, where $m_{C_\theta \to \Delta x_\theta}$ and $m_{C_\theta \to \Delta y_\theta}$ are the means of $\Delta x_{\hat{\theta}}$ and $\Delta y_{\hat{\theta}}$, respectively; $\sigma^2_{C_\theta \to \Delta x_\theta}$ and $\sigma^2_{C_\theta \to \Delta y_\theta}$ are the variances of $\Delta x_{\hat{\theta}}$ and $\Delta y_{\hat{\theta}}$, respectively. We derive the messages for (3) and (4), based on the formula for the product of two independent random variables $(a \cdot b)$ as [17]

$$m_{a \cdot b} = m_a \cdot m_b, \tag{5}$$

$$\sigma^2_{a \cdot b} = m_a^2 \cdot \sigma_b^2 + m_b^2 \cdot \sigma_a^2 + \sigma_a^2 \cdot \sigma_b^2, \tag{6}$$

where m_x and σ_x^2, $x \in \{a, b, a \cdot b\}$ are the mean and variance of x, respectively. It should be noticed from (3)–(6) that the means and variances of $\tan(\hat{\theta})$ and $\cot(\hat{\theta})$, $m_{\tan(\hat{\theta})}$ and $\sigma^2_{\tan(\hat{\theta})}$, $m_{\cot(\hat{\theta})}$ and $\sigma^2_{\cot(\hat{\theta})}$, respectively, are required. However, there arises a problem because $\tan(\hat{\theta})$ and $\cot(\hat{\theta})$ in (4) and (3) are both nonlinear functions that violates the Gaussianity assumption to express the messages only by the mean and variance in the FG. This motivates us to use the first-order TS to derive linear approximation of the tangent and cotangent functions to obtain the messages corresponding to the relative distance, as $(m_{C_\theta \to \Delta x_\theta}, \sigma^2_{C_\theta \to \Delta x_\theta})$ and $(m_{C_\theta \to \Delta y_\theta}, \sigma^2_{C_\theta \to \Delta y_\theta})$. The detailed derivation is described below.

The first-order TS is expressed as [18]

$$f(\hat{\theta}) \approx f\left(m_{\hat{\theta}}\right) + f'\left(m_{\hat{\theta}}\right)\left(\hat{\theta} - m_{\hat{\theta}}\right), \tag{7}$$

where $f(\hat{\theta})$ is either $\tan(\hat{\theta})$ or $\cot(\hat{\theta})$, $\hat{\theta}$ is the DOA sample, $m_{\hat{\theta}}$ is the mean of $\hat{\theta}$, $f(m_{\hat{\theta}})$ is either the $\tan(m_{\hat{\theta}})$ or $\cot(m_{\hat{\theta}})$, and $f'(m_{\hat{\theta}})$ is the first derivative of $f(m_{\hat{\theta}})$. It should be noticed that (7) is a linear approximation for function of $\hat{\theta}$, and hence, it is found that $f(\hat{\theta})$ can be approximated by a Gaussian variable. The mean $m_{f(\hat{\theta})}$ and variance $\sigma^2_{f(\hat{\theta})}$ can then be approximated using (7) as [18]

$$m_{f(\hat{\theta})} \approx f\left(m_{\hat{\theta}}\right), \tag{8}$$

$$\sigma^2_{f\left(\hat{\theta}\right)} \approx \left(f'\left(m_{\hat{\theta}}\right)\right)^2 \cdot \sigma^2_{\hat{\theta}}, \tag{9}$$

where $\sigma^2_{\hat{\theta}}$ is the variance of $\hat{\theta}$. The mean and variance of $\tan(\hat{\theta})$ and $\cot(\hat{\theta})$ are obtained from (8) and (9), respectively, as

$$m_{\tan(\hat{\theta})} \approx \tan\left(m_{\hat{\theta}}\right), \tag{10}$$

$$m_{\cot(\hat{\theta})} \approx \cot\left(m_{\hat{\theta}}\right), \tag{11}$$

$$\sigma^2_{\tan(\hat{\theta})} \approx \sec^4(m_{\hat{\theta}}) \cdot \sigma^2_{\hat{\theta}}, \tag{12}$$

$$\sigma^2_{\cot(\hat{\theta})} \approx \csc^4(m_{\hat{\theta}}) \cdot \sigma^2_{\hat{\theta}}. \tag{13}$$

Equations (11) and (13) provide our proposed algorithm with accurate enough approximation over a relatively large value range of the angles except for the mean of the angles around 0 radiant. This exception is because $\cot(0)$ and $\csc(0)$ are infinity. Hence, we can solve the infinity problem by empirically setting a limit value of m_θ. We found that $m_{\hat{\theta}} \geq |0.1|$ in units of radiant is reasonable. By setting the limit value properly, unstable behavior of the algorithm can be avoided. Theoretically, we also require to set a limit value of $m_{\hat{\theta}}$ for (10) and (12), (11) and (13) to avoid the infinity values for the angles around $\{\pi/2, 3\pi/2\}$, $\{2\pi\}$ radiants, respectively.

The node C_θ calculates relative distance messages, $(m_{C_\theta \to \Delta x_\theta}, \sigma^2_{C_\theta \to \Delta x_\theta})$ and $(m_{C_\theta \to \Delta y_\theta}, \sigma^2_{C_\theta \to \Delta x_\theta})$, according to (3)–(6) and (10)–(13), as

$$m_{C_\theta \to \Delta y_\theta} \approx m_{\Delta x_\theta \to C_\theta} \cdot \tan\left(m_{N_\theta \to C_\theta}\right), \tag{14}$$

$$m_{C_\theta \to \Delta x_\theta} \approx m_{\Delta y_\theta \to C_\theta} \cdot \cot\left(m_{N_\theta \to C_\theta}\right), \tag{15}$$

$$\begin{aligned} \sigma^2_{C_\theta \to \Delta y_\theta} \approx\ & \sigma^2_{\Delta x_\theta \to C_\theta} \cdot \tan^2\left(m_{N_\theta \to C_\theta}\right) \\ & + m^2_{\Delta x_\theta \to C_\theta} \cdot \sigma^2_{N_\theta \to C_\theta} \cdot \sec^4\left(m_{N_\theta \to C_\theta}\right) \\ & + \sigma^2_{\Delta x_\theta \to C_\theta} \cdot \sigma^2_{N_\theta \to C_\theta} \cdot \sec^4\left(m_{N_\theta \to C_\theta}\right), \end{aligned} \tag{16}$$

$$\begin{aligned} \sigma^2_{C_\theta \to \Delta x_\theta} \approx\ & \sigma^2_{\Delta y_\theta \to C_\theta} \cdot \cot^2\left(m_{N_\theta \to C_\theta}\right) \\ & + m^2_{\Delta y_\theta \to C_\theta} \cdot \sigma^2_{N_\theta \to C_\theta} \cdot \csc^4\left(m_{N_\theta \to C_\theta}\right) \\ & + \sigma^2_{\Delta y_\theta \to C_\theta} \cdot \sigma^2_{N_\theta \to C_\theta} \cdot \csc^4\left(m_{N_\theta \to C_\theta}\right). \end{aligned} \tag{17}$$

The node C_θ forwards the messages $(m_{C_\theta \to \Delta x_\theta}, \sigma^2_{C_\theta \to \Delta x_\theta})$ obtained from (15) and (17) to the *relative distance variable node* Δx_θ for the X-coordinate, while the messages $(m_{C_\theta \to \Delta y_\theta}, \sigma^2_{C_\theta \to \Delta y_\theta})$ obtained from (14) and (16) are forwarded to the *relative distance variable node* Δy_θ for the Y-coordinate. The variable node Δx_θ directly forwards the messages $(m_{\Delta x_\theta \to A_\theta}, \sigma^2_{\Delta x_\theta \to A_\theta})$ to the *relative distance factor node* A_θ, where $(m_{\Delta x_\theta \to A_\theta}, \sigma^2_{\Delta x_\theta \to A_\theta}) = (m_{C_\theta \to \Delta x_\theta}, \sigma^2_{C_\theta \to \Delta x_\theta})$. The node Δy_θ forwards the messages $(m_{\Delta y_\theta \to B_\theta}, \sigma^2_{\Delta y_\theta \to B_\theta})$ to the *relative distance factor node* B_θ, where $(m_{\Delta y_\theta \to B_\theta}, \sigma^2_{\Delta y_\theta \to B_\theta}) = (m_{C_\theta \to \Delta y_\theta}, \sigma^2_{C_\theta \to \Delta y_\theta})$.

The messages in the nodes A_θ and B_θ are finally converted to the coordinate variable node, as[6–8]

$$\left(m_{A_\theta \to \Delta x_\theta}, \sigma^2_{A_\theta \to \Delta x_\theta}\right) = \left(X - m_{x \to A_\theta}, \sigma^2_{x \to A_\theta}\right), \tag{18}$$

$$\left(m_{B_\theta \to \Delta y_\theta}, \sigma^2_{B_\theta \to \Delta y_\theta}\right) = \left(Y - m_{y \to B_\theta}, \sigma^2_{y \to B_\theta}\right), \tag{19}$$

$$\left(m_{A_\theta \to x}, \sigma^2_{A_\theta \to x}\right) = \left(X - m_{\Delta x_\theta \to A_\theta}, \sigma^2_{\Delta x_\theta \to A_\theta}\right), \tag{20}$$

$$\left(m_{B_\theta \to y}, \sigma^2_{B_\theta \to y}\right) = \left(Y - m_{\Delta y_\theta \to B_\theta}, \sigma^2_{\Delta y_\theta \to B_\theta}\right). \tag{21}$$

As shown in Fig. 2, the messages of (20) and (21), $(m_{A_\theta \to x}, \sigma^2_{A_\theta \to x})$ and $(m_{B_\theta \to y}, \sigma^2_{B_\theta \to y})$, produced by the nodes A_θ and B_θ, respectively, are forwarded to the *estimated target position variable nodes* x and y. According to the message-passing principle, now the reverse process is invoked. Recall that we omitted the sensor index in the equations; however, to derive the messages sent from the variable nodes x and y, the sensor index has to be introduced. All the messages coming from the nodes $A_{\theta_j}, j = \{1, ..., N\}$, except for the message sent back to the node A_{θ_i}, $i \neq j$, are used in the node x. It can be easily found by invoking the fact that the products of multiple Gaussian pdfs having different means and variances are proportional to the Gaussian pdf; the messages sent back from the variable node x to the factor node A_{θ_i} are given by $(m_{x \to A_{\theta_i}}, \sigma^2_{x \to A_{\theta_i}})$ as [5–8]

$$\frac{1}{\sigma^2_{x \to A_{\theta_i}}} = \sum_{j=1, j \neq i}^{N} \frac{1}{\sigma^2_{A_{\theta_j} \to x}}, \tag{22}$$

$$m_{x \to A_{\theta_i}} = \sigma^2_{x \to A_{\theta_i}} \cdot \sum_{j=1, j \neq i}^{N} \frac{m_{A_{\theta_j} \to x}}{\sigma^2_{A_{\theta_j} \to x}}, \tag{23}$$

where i and j are the sensor indexes. The messages $(m_{y \to B_{\theta_i}}, \sigma^2_{y \to B_{\theta_i}})$ can be obtained in the same way as $(m_{x \to A_{\theta_i}}, \sigma^2_{x \to A_{\theta_i}})$ calculated by (22) and (23).

The messages $(m_{x \to A_{\theta_i}}, \sigma^2_{x \to A_{\theta_i}})$ of (22) and (23) sent to the node A_{θ_i} are used by (18) to calculate the messages $(m_{A_{\theta_i} \to \Delta x_{\theta_i}}, \sigma^2_{A_{\theta_i} \to \Delta x_{\theta_i}})$, and in the same way, the messages $(m_{B_{\theta_i} \to \Delta y_{\theta_i}}, \sigma^2_{B_{\theta_i} \to \Delta y_{\theta_i}})$ are calculated by (19) using $(m_{y \to B_{\theta_i}}, \sigma^2_{y \to B_{\theta_i}})$. The messages $(m_{A_{\theta_i} \to \Delta x_{\theta_i}}, \sigma^2_{A_{\theta_i} \to \Delta x_{\theta_i}})$ of (18) are forwarded from the node A_{θ_i} to the node Δx_{θ_i}, and then, the messages $(m_{\Delta x_{\theta_i} \to C_{\theta_i}}, \sigma^2_{\Delta x_{\theta_i} \to C_{\theta_i}})$ are directly forwarded to the node C_{θ_i}, where $(m_{\Delta x_{\theta_i} \to C_{\theta_i}},$

$\sigma^2_{\Delta x_{\theta_i}\to C_{\theta_i}}) = (m_{A_{\theta_i}\to\Delta x_{\theta_i}}, \sigma^2_{A_{\theta_i}\to\Delta x_{\theta_i}})$. The messages $(m_{B_{\theta_i}\to\Delta y_{\theta_i}}, \sigma^2_{B_{\theta_i}\to\Delta y_{\theta_i}})$ of (19) are forwarded from the node B_{θ_i} to the node Δy_{θ_i}, and then, the messages $(m_{\Delta y_{\theta_i}\to C_{\theta_i}}, \sigma^2_{\Delta y_{\theta_i}\to C_{\theta_i}})$ are forwarded to the node C_{θ_i}, where $(m_{\Delta y_{\theta_i}\to C_{\theta_i}}, \sigma^2_{\Delta y_{\theta_i}\to C_{\theta_i}}) = (m_{B_{\theta_i}\to\Delta y_{\theta_i}}, \sigma^2_{B_{\theta_i}\to\Delta y_{\theta_i}})$. The entire process is repeated iteratively. When the iteration converges or maximum iteration is reached, all messages from the nodes A_{θ_i} and B_{θ_i} are combined in the nodes x and y as [5–8]

$$\frac{1}{\sigma_x^2} = \sum_{i=1}^{N} \frac{1}{\sigma^2_{A_{\theta_i}\to x}}, \tag{24}$$

$$\frac{1}{\sigma_y^2} = \sum_{i=1}^{N} \frac{1}{\sigma^2_{B_{\theta_i}\to y}}, \tag{25}$$

$$m_x = \sigma_x^2 \cdot \sum_{i=1}^{N} \frac{m_{A_{\theta_i}\to x}}{\sigma^2_{A_{\theta_i}\to x}}, \tag{26}$$

$$m_y = \sigma_y^2 \cdot \sum_{i=1}^{N} \frac{m_{B_{\theta_i}\to y}}{\sigma^2_{B_{\theta_i}\to y}}. \tag{27}$$

Finally, the estimated coordinate position (x, y) of the unknown radio wave emitter is determined by (m_x, m_y). To provide more comprehensive understanding, we summarize all equations operating at each node of the FG in Table 1, where the directions of the message flow is shown in the left column.

4 CRLB derivation for DOA-based geolocation

This section derives the CRLB for DOA-based geolocation, taking into account the number of samples. The CRLB for DOA-based geolocation is presented in [7]; however, it does not take into account the effect of number of samples. The likelihood for K i.i.d. samples $\hat{\theta}_k$, $k = \{1, 2, \ldots, K\}$, following the Gaussian distribution, is presented in [19], as

$$p(\hat{\theta};\theta) = \prod_{k=0}^{K-1} \frac{1}{\sqrt{2\pi\sigma_\theta^2}} \exp\left(-\frac{1}{2\sigma_\theta^2}\left(\hat{\theta}_k - \theta\right)^2\right),$$

where $\theta = \arctan\left(\frac{Y_i - y}{X_i - x}\right)$. Here, the sensor index i is omitted again for simplicity. After several mathematical manipulations, as described in the Appendix, the closed form of the second-order derivative of log-likelihood function (LLF) is expressed as [19]

$$\frac{\partial^2}{\partial\theta^2} \ln p(\hat{\theta};\theta) = -\frac{K}{\sigma_\theta^2}. \tag{28}$$

Table 1 The operations required for each node in the DOA-based TS FG

Nodes	Means, variances	
	Inputs	Outputs
$D_{\theta_i} \to N_{\theta_i}$	$\hat{\theta}_i$ samples	$m_{\hat{\theta}_i}, \sigma^2_{\hat{\theta}_i}$
$N_{\theta_i} \to C_{\theta_i}$	$m_{\hat{\theta}_i}, \sigma^2_{\hat{\theta}_i}$	$m_{\hat{\theta}_i}, \sigma^2_{\hat{\theta}_i}$
$C_{\theta_i} \to \Delta y_i$	m_i, σ_i^2 $m_{\hat{\theta}_i}, \sigma^2_{\hat{\theta}_i}$	$m_i \cdot \tan\left(m_{\hat{\theta}_i}\right)$, $\sigma_i^2 \cdot \tan^2\left(m_{\hat{\theta}_i}\right) + m_i^2 \cdot \sigma^2_{\hat{\theta}_i} \cdot \sec^4\left(m_{\hat{\theta}_i}\right)$ $+\sigma_i^2 \cdot \sigma^2_{\hat{\theta}_i} \cdot \sec^4\left(m_{\hat{\theta}_i}\right)$
$C_{\theta_i} \to \Delta x_i$	m_i, σ_i^2 $m_{\hat{\theta}_i}, \sigma^2_{\hat{\theta}_i}$	$m_i \cdot \cot\left(m_{\hat{\theta}_i}\right)$, $\sigma_i^2 \cdot \cot^2\left(m_{\hat{\theta}_i}\right) + m_i^2 \cdot \sigma^2_{\hat{\theta}_i} \cdot \csc^4\left(m_{\hat{\theta}_i}\right)$ $+\sigma_i^2 \cdot \sigma^2_{\hat{\theta}_i} \cdot \csc^4\left(m_{\hat{\theta}_i}\right)$
$C_{\theta_i} \leftarrow \Delta x_i \to A_{\theta_i}$ $C_{\theta_i} \leftarrow \Delta y_i \to B_{\theta_i}$	m_i, σ_i^2	m_i, σ_i^2
$\Delta x_i \leftarrow A_{\theta_i} \to x$	m_i, σ_i^2	$X_i - m_i, \sigma_i^2$
$\Delta y_i \leftarrow B_{\theta_i} \to y$	m_i, σ_i^2	$Y_i - m_i, \sigma_i^2$
$x \to A_{\theta_i}$ $y \to B_{\theta_i}$	m_j, σ_j^2 $j \neq i$	$\sigma_i^2 \sum_{j\neq i} \frac{m_j}{\sigma_j^2}, \sigma_i^2 = \frac{1}{\sum_{j\neq i}\frac{1}{\sigma_j^2}}$
x and y	m_i, σ_i^2	$\sigma^2 \sum_i \frac{m_i}{\sigma_i^2}, \sigma^2 = \frac{1}{\sum_i \frac{1}{\sigma_i^2}}$

The closed-form CRLB for DOA-based geolocation technique which takes into account the number of samples is found to be

$$\mathrm{CRLB}_{\mathrm{DOA}} = \sqrt{\mathrm{trace}\left(\left(\mathbf{J}^T \Sigma_\theta^{-1} \mathbf{J}\right) K\right)^{-1}}, \tag{29}$$

where $\Sigma_\theta = \sigma_\theta^2 \mathbf{I}_N$ denotes Gaussian covariance, $\mathbf{I}_N$ denotes an $N \times N$ identity matrix, and $\mathbf{J} = \frac{\partial \theta}{\partial \mathbf{x}}$ denotes Jacobian matrix given by

$$\mathbf{J} = \begin{bmatrix} \frac{Y_1 - y}{r_1^2} & -\frac{X_1 - x}{r_1^2} \\ \frac{Y_2 - y}{r_2^2} & -\frac{X_2 - x}{r_2^2} \\ \vdots & \vdots \\ \frac{Y_N - y}{r_N^2} & -\frac{X_N - x}{r_N^2} \end{bmatrix} \tag{30}$$

with the r_i denotes the Euclidean distance between the target and sensors.

5 Simulation results

The performance of the proposed technique was verified via computer simulations, where the simulation round consists of 1000 single-target locations randomly chosen from the area of 1000 × 1000 m^2, where each target location is tested in 100 trials. It should be noted here that the scope in this paper is to estimate only one target position. The case of unknown multiple-target detection is left for future work. It is assumed that the illegal radio, as an example of unknown radio emitter, emits the radio wave with strong enough transmit power covering the area of 1000 × 1000 m^2. The values of the measurement error were $\sigma_\theta = \{1°, 5°, 10°, 15°, \cdots, 45°\}$. It was assumed that the simulation does not contain outliers in angular measurement.

It may be difficult to *achieve* the LOS condition in areas with a size of 1000 × 1000 m^2 especially in (sub)urban environments. However, instead, we can include the error due to the non-LOS components to the variance of the measurement error as shown in [20, 21], where the variances are different between the sensors. For simplicity, we assume that the variance σ_θ^2 of the measurement error is common to all sensors as in [6–8, 10, 11]. It is rather straightforward to derive the algorithm where each sensor has different values of variances. In fact, in our simulation setup, the area size is much smaller than that used in other references, for example, the TOA-based FG in [[8], TOA/DOA-based FG in [6], DOA-based FG in [7], and TDOA-based FG in [10], where they consider a hexagonal area with a radius of 5 km. Furthermore, as found in the simulation results, the estimation accuracy is quite high even with relatively large variance, e.g., with standard deviation $\sigma_\theta = 45°$. This indicates that the assumption for the impact of the non-LOS components being represented by the measurement error variance is reasonable.

As shown in Fig. 3, six sensors were assumed in total, indicated by the Δ mark. The positions of the sensors in the simulation were limited to certain positions making a *sensing area* with three and five sensors at {(100, 0), (1100, 0), (600, −1000)} m and {(100, 0), (1100, 0), (600, −500), (100, −1000), (1100, −1100)} m, respectively. As described above, the target positions are randomly chosen inside the sensing 1000 × 1000 m^2 area to evaluate the effectiveness of the proposed technique.

The accuracy of the proposed technique was evaluated by using the following parameters: (a) three to five sensors taken from the total of six sensors, (b) 25 to 1000 samples, and (c) 10 times of iterations for each trial. The initialization point is set at (0, 0) for $m_{x \to A_\theta}$ and $m_{y \to B_\theta}$ and at (1, 1) for $\sigma^2_{x \to A_\theta}$ and $\sigma^2_{y \to B_\theta}$. It should be noted that the initialization point can be set arbitrarily inside the area of the expected target detection. Regardless of the target positions (1000 points tested), with the initialization of mean and variance being set at (0, 0) and (1, 1), respectively, the final estimate of the target position is quite accurate. Conversely, this observation should be understood in a way that the estimation result is less sensitive to the initial values.

To demonstrate the convergence property of the proposed technique, the trajectory of a detection trail is shown in Fig. 4. It shows clearly that the target position estimate successfully reaches the true target position at $(x, y) = (444, -746)$ m in 10 iterations, where the iteration process is started from the initial point (0,0) m. The estimate target position is calculated in each iteration by using (26) and (27). It should be noticed that only with seven iterations, the position estimate of the proposed technique reaches a point close to the true target position by using three sensors.

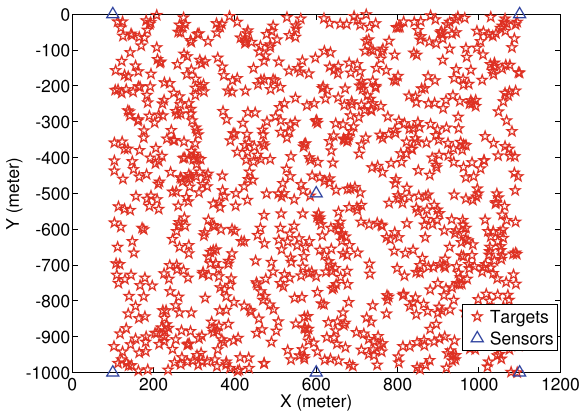

Fig. 3 1000 target and six sensor positions in area 1000 × 1000 m^2

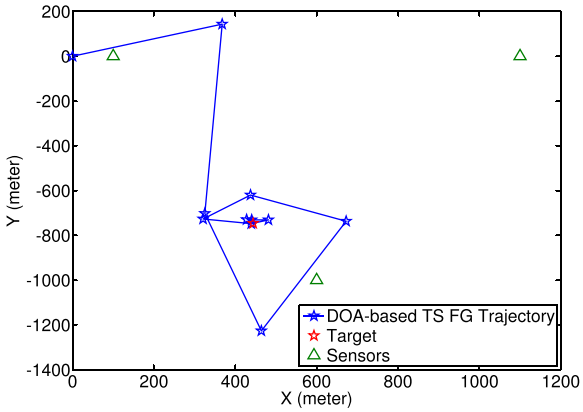

Fig. 4 Trajectory of the proposed technique with 3 sensors, 10 iterations, 100 samples, $\sigma_\theta = 10°$, and target at (444, −746) m

Figure 5 shows the RMSE versus the iteration times with the standard deviation σ_θ of the measurement error as a parameter. The RMSE of the proposed technique converges after nine iterations for $\sigma_\theta = 1°$, while it converges after five iterations for $\sigma_\theta = 20°$ and $\sigma_\theta = 45°$ as shown in Fig. 5. Hence, the iteration converges faster with a higher standard deviation of the measurement error because lower σ_θ needs more times to achieve better accuracy. Although the RMSE with $\sigma_\theta = 1°$ is worse with less than five iterations, the RMSE with smaller σ_θ is lower when the iterations converges.

To make a comparison of the accuracy of the proposed technique to the conventional DOA-based LS technique in [16], we conducted another series of the conventional DOA-based LS algorithm [16] in summarized below

$$\begin{bmatrix} m_{y_{\mathrm{LS}}} \\ m_{x_{\mathrm{LS}}} \end{bmatrix} = \left(A^T A\right)^{-1} A^T b, \tag{31}$$

where

$$A = \begin{bmatrix} 1 - \tan\left(m_{N_{\theta_1} \to C_{\theta_1}}\right) \\ 1 - \tan\left(m_{N_{\theta_2} \to C_{\theta_2}}\right) \\ \vdots \\ 1 - \tan\left(m_{N_{\theta_N} \to C_{\theta_N}}\right) \end{bmatrix}, \tag{32}$$

$$b = \begin{bmatrix} Y_1 - X_1 \tan\left(m_{N_{\theta_1} \to C_{\theta_1}}\right) \\ Y_2 - X_2 \tan\left(m_{N_{\theta_2} \to C_{\theta_2}}\right) \\ \vdots \\ Y_N - X_N \tan\left(m_{N_{\theta_N} \to C_{\theta_N}}\right) \end{bmatrix},$$

with $(m_{x_{\mathrm{LS}}}, m_{y_{\mathrm{LS}}})$ being the target position estimate. The RMSEs achieved by the proposed and the conventional DOA-based LS techniques are then compared with the CRLB. In each round of simulations, both techniques used the same parameter values as described before.

Figure 6 shows that the RMSE versus the standard deviation σ_θ of the measurement error with the number of sensors as a parameter. It is found that the more sensors, the smaller the RMSE. Figure 7 shows the number of the sensors versus the RMSE with the standard deviation σ_θ of the measurement error as a parameter. It is found from the figure that there is a clear difference in the tendency of the RMSE between the proposed technique and the conventional DOA-based LS technique. With the conventional DOA-based LS technique, the RMSE with three sensors yields better performance than that of with four sensors for $\sigma_\theta = 1°$, and the RMSE with five sensors is almost the same as that with four sensors. This indicates that since the LS equation is overdetermined with more than three sensors, the LS error is the dominant factor with $\sigma_\theta = 1°$. When $\sigma_\theta = \{20°, 45°\}$, on the other hand, the measurement error is the dominating factor, and hence,

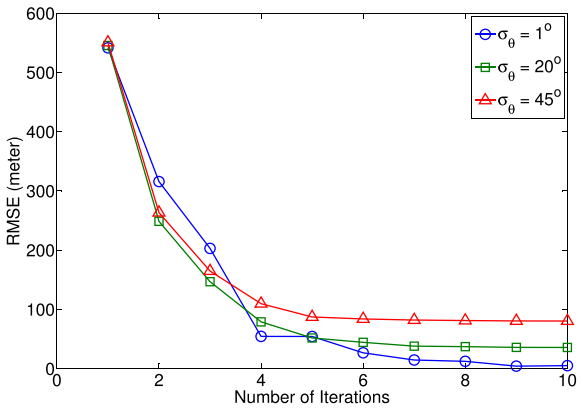

Fig. 5 RMSE vs. iteration times of DOA-based TS FG geolocation technique with 3 sensors, 10 iterations, 100 samples, 1000 locations, 100 trials, and $\sigma_\theta = \{1°, 20°, 45°\}$

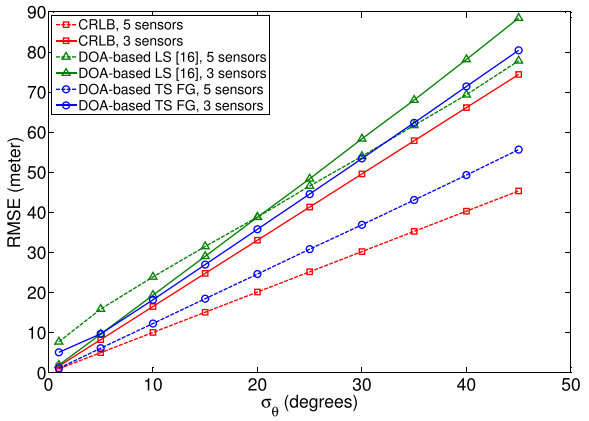

Fig. 6 RMSE vs. σ_θ with 3–5 sensors, 10 iterations, 100 samples, 1000 locations, and 100 trials

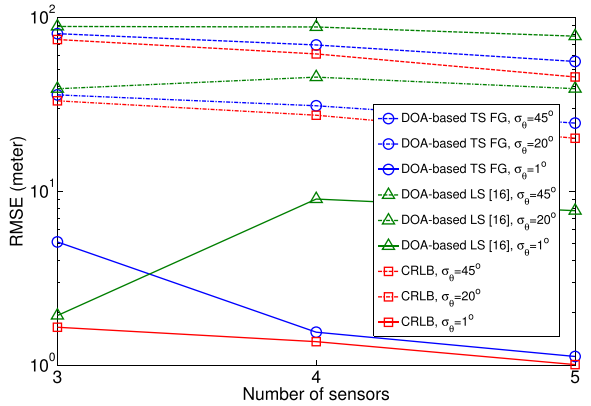

Fig. 7 RMSE vs. sensor number with 10 iterations, 1000 locations, 100 trials, and $\sigma_\theta = \{1°, 20°, 45°\}$

the achieved RMSEs with three, four, and five sensors are almost the same. This may be because the measurement error dominates the accuracy over the error due to the overdetermination.

In contrast to this observation, the RMSE decreases by increasing the sensor number for $\sigma_\theta = \{1°, 20°, \text{and } 45°\}$ with the proposed technique, and such tendency is consistent to the CRLB. It can be concluded that the geolocation accuracy in terms of RMSE with the proposed technique outperforms the reference conventional DOA-based LS technique.

Figure 8 shows the effect of the number of samples to the accuracy of DOA-based geolocation techniques with σ_θ as a parameter. The RMSE of both the proposed and reference techniques[16] as well as the CRLB for the DOA-based geolocation decreases when more samples are used. It is shown in Fig. 8 that with RMSE 24 m, the proposed technique requires around 525 samples, while the conventional technique requires around 630 samples.

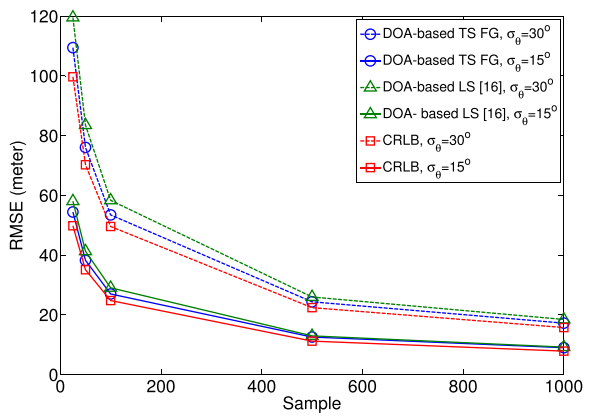

Fig. 8 RMSE vs. the number of samples with 3 sensors, 10 iterations, 1000 locations, 100 trials, and $\sigma_\theta = \{15°, 30°\}$

The accuracy of the proposed technique always outperforms the reference technique with the same number of samples used. Obviously, by increasing the number of samples, the gap to the CRLB decreases with both the proposed and reference techniques. It is also found from the figure that the smaller the measurement error, the smaller the gap to the CRLB. The gap with different σ_θ values decreases when the number of samples increases.

6 Conclusions

We have proposed a new FG-based geolocation technique using DOA information for a single unknown (anonymous) radio emitter with accuracy improvement of the position estimate. We have derived a set of new approximated expression for the mean and variance of the tangent and cotangent functions based on the first-order TS to hold the Gaussianity assumption. We have also derived a closed-form expression of the CRLB for DOA-based techniques taking into account the influence of the number of samples. The simulation results confirmed that our proposed technique provides (a) better accurate position estimate with the number of samples, number of sensors, and standard deviation of measurement error as parameters, (b) fast convergence, and (c) keep low computational complexity, which are suitable for the future geolocation techniques requiring high accuracy and low complexity in an imperfect synchronization condition. The development of DOA-based TS FG technique for multiple-target detection is left as future work.

Appendix: CRLB derivations for DOA-based geolocation

The sensor index i is omitted in this derivation for simplicity. By taking the expectation of (28), we have

$$E\left[\frac{\partial^2}{\partial\theta^2}\ln p(\hat{\theta};\theta)\right] = -\frac{K}{\sigma_\theta^2}. \tag{33}$$

Since

$$E\left[\left(\frac{\partial}{\partial\theta}\ln p\left(\hat{\theta};\theta\right)\right)^2\right] = -E\left[\frac{\partial^2}{\partial\theta^2}\ln p\left(\hat{\theta};\theta\right)\right], \tag{34}$$

as shown in [19]

$$E\left[\left(\frac{\partial}{\partial\theta}\ln p(\hat{\theta};\theta)\right)^2\right] = \frac{K}{\sigma_\theta^2}. \tag{35}$$

The Fisher information matrix (FIM) [19, 22, 23]

$$\mathbf{F}(\mathbf{x}) = \frac{\partial\theta}{\partial\mathbf{x}}^T E\left[\left(\frac{\partial}{\partial\theta}\ln p(\hat{\theta};\theta)\right)^T\left(\frac{\partial}{\partial\theta}\ln p(\hat{\theta};\theta)\right)\right]\frac{\partial\theta}{\partial\mathbf{x}} \tag{36}$$

is found to

$$\mathbf{F}(\mathbf{x}) = \frac{\partial\theta}{\partial\mathbf{x}}^T E\left[\left(\frac{\partial}{\partial\theta}\ln p(\hat{\theta};\theta)\right)^2\right]\frac{\partial\theta}{\partial\mathbf{x}}. \tag{37}$$

Substituting (35) into (37) yields

$$\mathbf{F}(\mathbf{x}) = \frac{\partial\theta}{\partial\mathbf{x}}^T \left[\frac{K}{\sigma_\theta^2}\right] \frac{\partial\theta}{\partial\mathbf{x}}. \tag{38}$$

Now, we replace θ by a vector $\theta = (\theta_1, \ldots, \theta_N)$. Then, the variance (σ_θ^2) is replaced by the Gaussian covariance matrix Σ_θ, as

$$\mathbf{F}(\mathbf{x}) = K\mathbf{J}^T \Sigma_\theta^{-1} \mathbf{J}. \tag{39}$$

Finally, by substituting (39) into the CRLB expression (29), as in [7, 10, 19], we obtain the CRLB for a DOA-based geolocation technique that takes into account the measured number of samples K, as

$$\mathrm{CRLB}_{\mathrm{DOA}} = \sqrt{\mathrm{trace}\left(\left(\mathbf{J}^T \Sigma_\theta^{-1} \mathbf{J}\right) K\right)^{-1}}.$$

Acknowledgements
This research is supported, in part, by Koden Electronics Co., Ltd., and in part by the Doctor Research Fellow (DRF) Program of Japan Advanced Institute of Science and Technology (JAIST).

Authors' contributions
MRKA conceived and designed the research work, expanded and improved the algorithms for more potential applications, conducted computer simulations, acquired and analyzed data, and critically revised the manuscript. KA conceived and designed the research work, developed the base of algorithm for geolocation, analyzed data, and critically revised the manuscript. TM conceived and designed the research work, performed verification of the algorithm, analyzed data, and critically revised the manuscript. All authors read and approved the final manuscript.

Competing interests
The authors declare that they have no competing interests.

Author details
[1]School of Information Science, Japan Advanced Institute of Science and Technology (JAIST), 1-1 Asahidai, Nomi-shi 923-1292, Japan. [2]Electrical Enginering Department, Institut Teknologi Sumatera (ITERA), Lampung Selatan 35365, Indonesia. [3]Centre for Wireless Communications (CWC), University of Oulu, 90014 Oulu, Finland.

Received: 25 April 2015 Accepted: 5 August 2016
Published online: 18 August 2016

References

1. J James, J Caffery, GL Stuber, Overview of radiolocation in CDMA cellular systems. IEEE Commun. Mag. **36**(4), 38–45 (1998)
2. K Pahlavan, X Li, J-P Makela, Indoor geolocation science and technology. IEEE Commun. Mag. **40**, 112–118 (2002)
3. Y Zhao, Standardization of mobile phone positioning for 3G systems. IEEE Commun. Mag. **40**, 108–116 (2002)
4. J-C Chen, C-S Maa, J-T Chen, in *Proc. IEEE International Conference on Acoustics, Speech, and Signal Processing (ICASSP) 2003*. Factor graphs for mobile position location, vol. 2, (2003), pp. 393–396
5. FR Kschischang, BJ Frey, H-A Loeliger, Factor graphs and the sum-product algorithm. IEEE Trans. Inf. Theory. **47**(2), 498–519 (2001)
6. J-C Chen, P Ting, C-S Maa, J-T Chen, in *IEEE VTC 2004*. Wireless geolocation with TOA/AOA measurements using factor graph and sum-product algorithm, vol. 5, (2004), pp. 3526–3529
7. B Omidali, SA-AB Shirazi, in *14th International CSI Computer Conference (CSICC 2009)*. Performance improvement of AOA positioning using a two-step plan based on factor graphs and the Gauss-Newton method, (2009), pp. 305–309
8. J-C Chen, Y-C Wang, C-S Maa, J-T Chen, Network side mobile position location using factor graphs. IEEE Trans. Wireless Comm. **5**(10), 2696–2704 (2006)
9. J-C Chen, C-S Maa, J-T Chen, Mobile position location using factor graphs. IEEE Commun. Lett. **7**, 431–433 (2003)
10. C Mensing, S Plass, Positioning based on factor graphs. EURASIP J. Adv. Signal Process. **2007**(ID 41348), 1–11 (2007)
11. C-T Huang, C-H Wu, Y-N Lee, J-T Chen, A novel indoor RSS-based position location algorithm using factor graphs. IEEE Trans. on Wireless Comm. **8**(6), 3050–3058 (2009)
12. G Giorgetti, A Cidronali, SKS Gupta, G Manes, Single-anchor indoor localization using a switched-beam antenna. Commun. Letters, IEEE. **13**(1), 58–60 (2009)
13. J Wang, J Chen, D Cabric, Cramer-Rao bounds for joint RSS/DOA-based primary-user localization in cognitive radio networks. IEEE Trans. Wireless Commun. **12**(3), 1363–1375 (2013)
14. DG Gregoire, GB Singletary, in *Aerospace and Electronics Conference, 1989. NAECON 1989., Proceedings of the IEEE 1989 National*. Advanced ESM AOA and location techniques, (1989), pp. 917–9242
15. SZ Kang, Z Ming, in *Aerospace and Electronics Conference, 1988. NAECON 1988., Proceedings of the IEEE 1988 National*. Passive location and tracking using DOA and TOA measurements of single nonmaneuvering observer, (1988), pp. 340–3441
16. P Kulakowski, J Vales-Alonsob, E Egea-Lopez, W Ludwin, J Garcá-Haro, Angle-of-arrival localization based on antenna arrays for wireless sensor networks. Comput. Electr. Eng. **36**, 1181–1186 (2010)
17. N O'Donoughue, JMF Moura, On the product of independent complex Gaussians. IEEE Trans. Signal Process. **60**(3), 1050–1063 (2012)
18. G Casella, RL Berger, *Statistical inference*, 2nd edn., (Duxbury, 2002)
19. SM Kay, *Fundamentals of statistical signal processing: estimation theory*. (Prentice Hall, 1993)
20. H-L Jhi, J-C Chen, C-H Lin, A factor-graph-based TOA location estimator. IEEE Commun. Mag. **11**(5), 1764–1773 (2012)
21. MP Wylie, J Holtzman, The non-line of sight problem in mobile location estimation. IEEE Trans. Signal Process, 827–831 (1996)
22. C Gentile, N Alsindi, R Raulefs, C Teolis, *Geolocation techniques, principles and applications*. (Springer, New York, 2013)
23. G Mao, B Fidan, *Localization algorithms and strategies for wireless sensor networks: monitoring and surveillance techniques for target tracking*. (IGI Global, New York, 2009)